

HYPERNUCLEAR PHYSICS WITH PHOTONS*

C. Bennhold^{a,b}, T. Mart^{c,b}, F.X. Lee^a, H. Haberzettl^a, H. Yamamura^d, K. Miyagawa^d,
W. Glöckle^e, S.S. Kamalov^{f,b}, L. Tiator^b, L.E. Wright^g

^a *Center for Nuclear Studies, Department of Physics, George Washington University, Washington, D.C. 20052, USA*

^b *Institut für Kernphysik, Johannes Gutenberg-Universität, 55099 Mainz, Germany*

^c *Jurusan Fisika, FMIPA, Universitas Indonesia, Depok 16424, Indonesia*

^d *Department of Applied Physics, Okayama University of Science 1-1 Ridai-cho, Okayama 700, Japan*

^e *Institut für Theoretische Physik II, Ruhr-Universität Bochum, D-44780 Bochum, Germany*

^f *Laboratory of Theoretical Physics, JINR Dubna, SU-101000, Moscow, Russia*

^g *Department of Physics, Ohio University, Athens, Ohio 45701, USA*

Abstract

We review the opportunities and challenges in the field of hypernuclear physics with electromagnetic probes. An overview is presented regarding our current understanding of the elementary production process on the nucleon. This amplitude is then used in the nuclear environment to study the hyperon-nucleon (YN) interaction. We discuss two scenarios: hypernuclear excitation that allows the investigation of hypernuclear structure and the bound Λ in the nucleus, and quasifree kaon production on the deuteron and on nuclei, which permits a more direct access to the YN force. Specific examples are given for few-body systems and shell-model nuclei.

1 ELEMENTARY KAON PHOTOPRODUCTION ON THE NUCLEON

Since we are still a long way from calculating the scattering and electromagnetic production of mesons on baryons directly from QCD, effective field-theoretical descriptions in terms of purely hadronic degrees of freedom are usually employed to compute such processes. QCD is assumed to provide the justification for the parameters or cutoff functions used in the various approaches. At threshold, SU(2) Chiral Perturbation Theory has been moderately successful to describe pion photo- and electroproduction; attempts to expand these techniques into the SU(3) arena to eta and kaon production are still in their infancy. In the resonance region one usually relies on effective Lagrangian approaches where a potential or driving term is defined that includes standard nonresonant s -, t -, and u -channel poles along with resonances in each of these channels as bare fields which are then dressed through the final-state interaction. Only the dressed s -channel poles above threshold are identified with physical resonances, the nonpolar part is considered background for the particular process (even though it may contain bare baryon resonances in the u -channel).

*Keynote talk at the JLab workshop on Hypernuclear Physics with Electromagnetic Probes (HYPLAB99), Jefferson Lab, Dec. 2-4, 1999

While dynamical models involving various approximations for the Bethe-Salpeter equation are becoming increasingly successful in the description of pion photoproduction, the hadronic final state interaction in kaon photoproduction has usually been neglected. Without rescattering contributions the T -matrix is simply approximated by the driving term alone which is assumed to be given by a series of tree-level diagrams [1, 2, 3, 4, 5, 6]. Clearly, neglecting the final meson-baryon interaction in the full meson photoproduction T -matrix automatically leads to violation of unitarity since flux that can "leak out" into inelastic channels has not been properly accounted for. Enforcing unitarity dynamically requires solving a system of coupled channels with all possible final states.

The most recent coupled-channels approach within an effective Lagrangian framework has been developed by Feuster and Mosel [7, 8] and extended to higher energies and additional channels by Waluyo *et al.* [9]. Nucleon resonance parameters are extracted by simultaneously analyzing all available data for reactions involving the initial and final states γN , πN , $\pi\pi N$, ηN , $K\Lambda$, $K\Sigma$ and $\eta'N$ up to $W = 2.0$ GeV. The calculations employ the K -matrix approximation, placing both intermediate particles on their mass shell. This procedure still allows for the resonance widths to be generated dynamically, while the real part of the self-energy is absorbed in an effective resonance mass that is determined by the fit.

1.1 The Born terms: SU(3) coupling constants, form factors and gauge invariance

Our understanding of the kaon-baryon interaction is still much poorer than our knowledge of the pion-nucleon force, exemplified by the uncertainty in the kaon-hyperon-nucleon coupling constants $g_{K\Lambda N}$ and $g_{K\Sigma N}$. Unlike the well established pion-nucleon interaction which yields a pion-nucleon coupling constant $g_{\pi NN}^2/4\pi$ around 13.7, the kaon coupling constants extracted from different reactions (from hadronic to electromagnetic) have much larger uncertainties, as shown in Table 1. Most isobar models for kaon photoproduction over the last 30 years have left the leading KYN couplings as open parameters to be determined by the data. Constraining these values to within the SU(3) range gave results which were overpredicting the data by up to a factor of 10. Therefore, when left as free parameters the couplings came out to be significantly smaller than the SU(3) range. On the other side, most extractions based on hadronic reactions yielded couplings constants well within the SU(3) limits. This discrepancy suggested that an important piece of physics has been left out in isobar models: the extended structure of the hadrons, parametrized in terms of a hadronic form factor.

However, it is well-known that the sum of the first three photoproduction diagrams—i.e., the sum of the s -, u -, and t -channel diagrams—is gauge-invariant only for bare hadronic vertices with pure pseudoscalar coupling. Thus, for this most basic case, the addition of a fourth contact-type graph is not necessary for preserving gauge invariance. In all other instances, however, one needs additional currents to ensure gauge invariance and thus current conservation. For bare hadronic vertices with pseudovector coupling, this extra current is the well-known Kroll-Ruderman contact term.

Irrespective of the coupling type, however, most isobaric models with bare vertices show a divergence at higher energies, which clearly points to the need for introducing hadronic form factors to cut off this undesirable behavior. For example, recent calculations [1, 3] demonstrated that many models which are able to describe (γ, K^+) experimental data tend to unrealistically overpredict the (γ, K^0) channel. The use of point-like particles disregards the composite nature

Table 1: The Born coupling constants obtained from various sources.

Source	$\frac{g_{K\Lambda N}}{\sqrt{4\pi}}$	$\frac{g_{K\Sigma N}}{\sqrt{4\pi}}$	Reference
SU(3)	-4.40 to -3.0	+0.9 to +1.3	[10]
K - N scattering	3.53	1.53	[11]
Y - N scattering	-3.86	+1.09	[12]
$N\bar{N} \rightarrow Y\bar{Y}$ LEAR data	-3.92	-	[12]
QCD sum rules	-2.82 to -1.96	0.25 to 0.80	[13, 14]
$\gamma p \rightarrow K^+\Lambda(\Sigma)$ (extrapolation)	3.52	-	[15]
$\gamma p \rightarrow K^+\Lambda(\Sigma)$ (isobar models)	-4.2 to -0.9	+0.02 to 1.8	many

of nucleons and mesons, thus losing the full complexity of a strongly interacting hadronic system.

To provide the desired higher-energy fall-off and still preserve the gauge invariance of the bare tree graphs, some models introduce a cut-off function and multiply the entire photoproduction amplitude with an overall function of monopole form,

$$F(\Lambda, t) = \frac{\Lambda^2 - m_K^2}{\Lambda^2 - t} \quad \text{or} \quad F(\Lambda, \mathbf{q}^2) = \frac{\Lambda^2 - m_K^2}{\Lambda^2 - \mathbf{q}^2} \quad (1)$$

where the cut-off mass Λ is treated as a free parameter. In spite of successfully minimizing the χ^2 while maintaining gauge invariance, there is no microscopic basis for this approach.

Field theory clearly mandates that a correct description of vertex dressing must be done in terms of individual hadronic form factors for each of the three kinematic situations given by the s -, u -, and t -channel diagrams. In a complete implementation of a field theory, the gauge invariance of the total amplitude is ensured by the self-consistency of these dressing effects, by additional interaction currents and by the effects of hadronic scattering processes in the final state [16]. Schematically, the interaction currents and the final-state contributions can always be written in the form of an additional contact diagram. If one now seeks to describe the dressing of vertices on a more accessible, somewhat less rigorous, level, one introduces phenomenological form factors for the individual s -, u -, and t -channel vertices. Then, to ensure gauge invariance and to remain close to the topological structure of the full underlying theory, the simplest option is to add contact-type currents which mock up the effects of the interaction currents and final-state scattering processes. In addition to the hadronic form factors multiplying the s -, u -, and t -channel diagrams, the longitudinal pieces of the gauge-invariance-preserving additional currents are only determined up to an arbitrary function \tilde{F} . For practical purposes, one of the simplest choices [16, 17] for this arbitrary function \tilde{F} has been taken to be a linear combination of the form factors for the three kinematic situations in which the dressed vertices appear, i.e.,

$$\begin{aligned} \tilde{F} &= a_s F(\Lambda, s) + a_u F(\Lambda, u) + a_t F(\Lambda, t), \\ &\text{with } a_s + a_u + a_t = 1, \end{aligned} \quad (2)$$

which introduces two more free parameters to be determined by fits to the experimental data. This method allows fixing the KYN couplings to the (approximate) SU(3) values and has

proven to be flexible and adequate for a good phenomenological description of experimental data. It has been used in all modern studies on kaon photoproduction in an effective Lagrangian framework [4, 8, 17]. Ultimately, high-quality data should allow an extrapolation to a Born term pole, possibly via dispersion relations, and an extraction of the $g_{K\Lambda N}$ and $g_{K\Sigma N}$ coupling constants. A precise determination of these coupling constants is especially important in view of the fact that the $g_{\eta NN}$ coupling appears to be much smaller than its SU(3) symmetry value [18].

1.2 Vector mesons in the t -channel

From pion photo- and electroproduction it is well known that for an adequate description of these electromagnetic processes the vector meson t -channel contributions play an important role as part of the background. Especially for the $p(\gamma, \pi^0)p$ reaction the ω meson is known to be an essential dynamical ingredient. Similarly, the equivalent vector meson with strangeness, the $K^*(892)$, has been included in the description of kaon photoproduction from the beginning. It was not until 1988, that the pseudovector meson $K_1(1270)$ was identified as also having an important effect in model fitting [19]. Similar non-strange pseudovector mesons [the $h_1(1170)$ and the $b_1(1235)$ states] have never been found to be important in pion photoproduction. One problem with the standard vector meson contributions in an effective Lagrangian framework is their divergence at energies beyond $W = 2.2\text{--}2.5$ GeV. This is the energy region which is ruled by Regge theory which starts from a description of t -channel Regge trajectory exchanges at forward angles. These trajectories represent the exchange of a family of mesons with the same internal quantum numbers and allow a natural description of the smooth energy and angular dependence observed in the data at high W . Reference [20] has recently applied this approach to high-energy pion and kaon photoproduction by replacing the usual pole-like Feynman propagator of a single particle exchanged in the t -channel by the so-called Regge propagator while keeping the vertex structure given by the effective Lagrangian for the ground state meson of the trajectory. For the transition region between s -channel resonance excitation and t -channel Regge exchange, duality would demand that exchanges are limited to either all s -channel or all t -channel contributions. In practice, however, since no resonance model ever includes all s -channel N^* states the vector mesons must be included as part of the background in some form.

1.3 Hyperon resonances in the u -channel

Crossing symmetry requires that the same amplitude which describes the $p(\gamma, K^+)\Lambda$ reaction should be able to describe the radiative capture process $p(K^-, \gamma)\Lambda$, when the Mandelstam variables s and u are interchanged. Due to SU(3) symmetry breaking crossing symmetry in a rigorous sense cannot be maintained since nucleons and hyperons have different excitation spectra. Some studies [1, 2] have applied a weaker crossing constraint by including selected hyperon resonances in the u -channel of the $p(\gamma, K^+)\Lambda$ reaction and fitting the radiative capture rate, $p(K^-, \gamma)\Lambda$, for kaons at rest along with the $p(\gamma, K^+)\Lambda$ data. Since hyperon resonances propagate in the s -channel in radiative kaon capture this process would be an excellent tool to constrain Y^* properties. In practice, only the capture rate at threshold has been measured; the energy dependence of this process is unknown. On the other hand, since hyperon resonances propagate in the u -channel in $p(\gamma, K^+)\Lambda$ they contribute to the background sector - and not to the resonance sector - of the kaon photoproduction process. Because of the remaining un-

certainties in the background other studies [3, 7, 8, 6] have refrained from including hyperon resonances.

1.4 *S*-channel Resonances: missing or otherwise

One of the most contentious issues in the phenomenological description of kaon photoproduction on the nucleon has been the choice of s-channel nucleon resonances in the production amplitude. Many studies have selected resonances that contribute to the kaon photoproduction process by their relative contribution to the overall χ^2 of the fit [1, 2, 3, 4]. Since this is usually done in tree-level calculations connections with other reaction channels are difficult to establish. As a consequence, some studies find large couplings of the $K\Lambda$ channel to spin 5/2 resonances, even though neither recent coupled-channels analyses [8, 21, 22] nor older partial-wave analyses for pionic $K\Lambda$ production [23, 24] give any indication that such states are important. It is the result of these multichannel analyses [7, 8, 21, 22] that inform us of the most important resonances decaying into $K\Lambda$ and $K\Sigma$ final states with a significant branching ratio. In the low-energy regime the dominant resonances for the $K\Lambda$ channel have been identified as the $S_{11}(1650)$, the $P_{11}(1710)$, and the $P_{13}(1720)$ states. For the $K\Sigma$ channel, the $S_{11}(1650)$ lies below threshold and the dominant states are *p*-wave: the $P_{11}(1710)$ and the $P_{13}(1720)$. At higher energies around $W = 1990$ MeV $K\Sigma$ production (both with photons and pions) appears to be dominated by the $T = 3/2$ states $S_{31}(1900)$ and $P_{31}(1910)$.

For the $p(\gamma, K^+)\Lambda$ channel the new SAPHIR total cross section data [25] indicate for the first time a structure around $W = 1900$ MeV that could not be resolved before due to the low quality of the old data. According to the Particle Data Book [26], only the 2-star $D_{13}(2080)$ has been identified in older $p(\pi^-, K^0)\Lambda$ analyses [23] as having a noticeable branching ratio into the $K\Lambda$ channel. On the theoretical side, the constituent quark model by Capstick and Roberts [27] predicts many new states around 1900 MeV; however, only a few them have been calculated to have a significant $K\Lambda$ decay width [28] and only one, the $[D_{13}]_3(1960)$, is also predicted to have significant photocouplings [30]. As discussed in more detail in Ref. [29], fits performed in an isobar model lead to remarkable agreement, up to the sign, between the quark model prediction and our extracted results for the $D_{13}(1960)$. Table 2 compares the extracted with the predicted resonance widths not only for this "missing" (?) state but also for the three states at lower energy. Ultimately, only a multipole analysis will be able to unambiguously identify the resonances contributing to kaon photoproduction. Due to the number of double polarization observables accessible because of the self-analyzing nature of the final hyperons a complete experiment for this reaction may be within reach.

1.5 An effective tree-level operator for nuclear applications

While it is generally recognized that a detailed understanding of the various reactions participating in resonance production must take place within a multichannel framework, these amplitudes are much too cumbersome to use in the nuclear environment. Nuclear calculations of pion, eta or kaon photoproduction usually need amplitudes that are easy to incorporate, have a straightforward off-shell extension, can be boosted to different Lorentz frames and are fast in terms of computer time. This is especially true for few-body calculations where high-dimensional integrals are solved in momentum space, requiring the subroutine for the elementary operator to be used on the order of 10^6 times. For this purpose the elementary amplitude is then parameterized

Table 2: Comparison between the extracted fractional decay widths and the result from the quark model [28, 30] for the $S_{11}(1650)$, $P_{11}(1710)$, $P_{13}(1720)$ and the "missing" $D_{13}(1900)$ resonances.

Resonance	$\sqrt{\Gamma_{N^*N\gamma}\Gamma_{N^*K\Lambda}}/\Gamma_{N^*}$ (10^{-3})	
	Extracted	Quark Model
$S_{11}(1650)$	-4.826 ± 0.051	-4.264 ± 0.984
$P_{11}(1710)$	1.029 ± 0.172	-0.535 ± 0.115
$P_{13}(1720)$	$1.165^{+0.041}_{-0.039}$	-1.291 ± 0.240
$D_{13}(1900)$	$2.292^{+0.722}_{-0.204}$	-2.722 ± 0.729

in a form that makes it easy to use, describes the elementary data well and preserves as many of the field-theoretical constraints as possible. In general, this involves constructing a tree-level amplitude, selecting a limited number of resonances which have been shown to be significant by multichannel analyses and refitting the coupling constants to the experimental data. Work over the last several years has shown that restoring gauge invariance in the presence of form factors is straightforward at the tree level. However, neglecting the final meson-baryon interaction in the meson photoproduction amplitude automatically leads to a violation of unitarity which is more difficult to restore. One possibility is to allow for energy-dependent phases for each multipole, as is done in the Mainz MAID pion electroproduction isobar model [31]. Furthermore, imposing dispersion relations would help to establish the proper analyticity properties of such effective amplitudes. No such attempts have yet been done for kaon photo- and electroproduction.

2 HYPERNUCLEAR EXCITATION

With the recent successful completion of the Jlab Hall C experiment 89-009 [32] which produced discrete hypernuclear states with electrons for the first time, the exploration of hypernuclear structure through electromagnetic probes is becoming a reality. In contrast to the hadronic reactions (K^-, π^-) and (π^+, K^+), the (γ, K^+) process uses, besides the photon, the rather weakly interacting K^+ with its mean free path of 5-7 fm in the nuclear medium, allowing the process to occur deep in the nuclear interior. In comparison, the K^- and the π^\pm are both strongly absorbed, thereby confining the reaction to the nuclear periphery. Due to the mass difference in the incoming kaon and outgoing pion, the (K^-, π^-) reaction allows for recoilless Λ production in the nucleus, leading to high counting rates. Kaon photoproduction, on the other hand, involves high momentum transfers due to the large production of the rest mass which will therefore project out high momentum components of the nuclear wave functions. Figure 1 illustrates the differences between the (K^-, π^-), (π^+, K^+), and (γ, K^+) production reactions, both in terms of their relative excitation strength and in terms of the structure of the produced hypernuclear spectrum for p-shell hypernuclei. At a strength of several 100 mb/sr the (K^-, π^-) reaction predominantly excites natural parity states with low angular momentum, such as the ground state $(p_{3/2,\Lambda}^{-1} s_{1/2})1^-$ or the substitutional state $(p_{3/2,\Lambda}^{-1} p_{3/2})0^+$. Reduced by about a factor of 50 in cross section, the (π^+, K^+) reaction still excites natural parity levels, but selecting the ones with large angular momentum, such as the $(p_{3/2,\Lambda}^{-1} p_{3/2})2_1^+$ and $(p_{3/2,\Lambda}^{-1} p_{1/2})2_2^+$

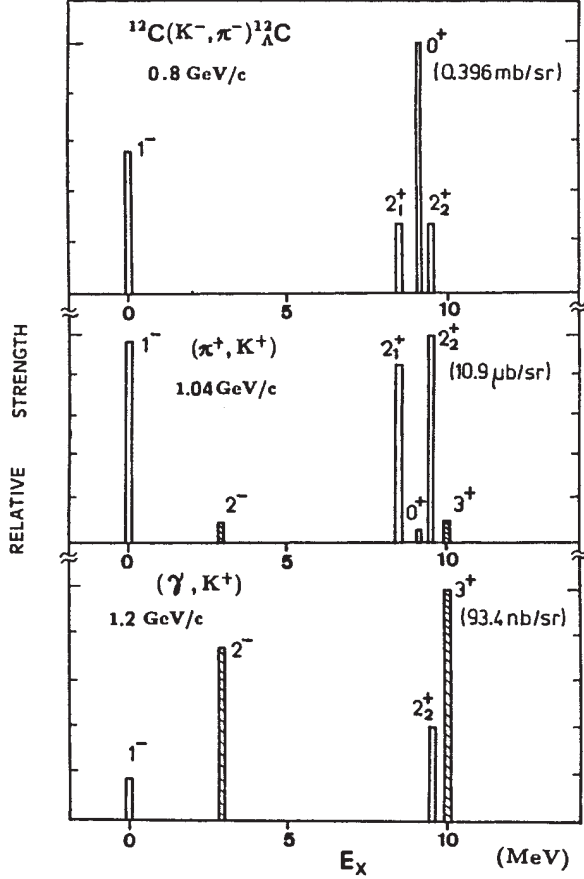


FIG. 1: Comparison of the theoretical excitation spectra for the reactions (K^-, π^-) , (π^+, K^+) and (γ, K^+) , producing ${}^{12}_{\Lambda}\text{C}$ (${}^{12}_{\Lambda}\text{B}$) at $\Theta_K = 10^\circ$. The 1^- and 2^- states belong to the ground state configuration $(p_{3/2, \Lambda}^{-1} s_{1/2})1^-, 2^-$ while the levels around $E_x=10$ MeV correspond to a Λ in a $p_{3/2}$ or $p_{1/2}$ orbit with levels $(p_{3/2, \Lambda}^{-1} p_{3/2})0^+, 1_1^+, 2_1^+, 3^+$ and $(p_{3/2, \Lambda}^{-1} p_{1/2})1_2^+, 2_2^+$. Only the strongly excited states are shown. This figure is taken from Ref. [35].

states, reflecting the larger momentum transfer of the process. Finally, the (γ, K^+) reaction excites primarily the unnatural parity, high angular momentum states, such as the ground state $(p_{3/2, \Lambda}^{-1} s_{1/2})2^-$ or the substitutional state $(p_{3/2, \Lambda}^{-1} p_{3/2})3^+$, albeit with a strength reduced by another two orders of magnitude, as one would expect for the electromagnetic interaction. This comparison demonstrates that full spectroscopic information can only be obtained with a combination of all three techniques. The subject of exciting discrete hypernuclear states through kaon photoproduction was studied extensively about 8-10 years ago [5, 6, 33, 34] but has been mostly dormant for the last several years, awaiting data taking. Therefore, the number of planned and approved experiments to take place within the next few years is expected to revive interest in this field.

2.1 Matrix elements for the process $\gamma + \Lambda \rightarrow K^+ + {}_{\Lambda}\text{B}$

As shown in detail in Ref. [5], assuming a one-body kaon photoproduction operator, the many-body nuclear matrix element naturally separates into a nuclear structure piece and a single-particle piece:

$$\langle J_f M_f; K^+ | T | J_i M_i; \gamma \rangle = \sum_{\alpha, \alpha'} \langle J_f M_f; K^+ | C_{\alpha'}^\dagger C_{\alpha} | J_i M_i; \gamma \rangle \langle \alpha'; K^+ | t | \alpha; \gamma \rangle. \quad (3)$$

In Eq. (3) the many-body nuclear structure aspects are separated from the photoproduction mechanism but in principle the sum extends over a complete set of single-particle states α and α' . The nuclear structure information involved in one-body processes is usually contained in the reduced density matrix elements (RDME),

$$\Psi_J(a', a) = \hat{J}^{-1} \langle J_f | [C_{\alpha'}^\dagger \otimes C_\alpha] | J_i \rangle . \quad (4)$$

All the dynamics of the photoproduction process is contained in the single-particle matrix element $\langle \alpha'; K^+ | t | \alpha; \gamma \rangle$ which in general involves a nonlocal operator. In momentum space this matrix element has the form

$$\langle \alpha'; K^+ | t | \alpha; \gamma \rangle = \int d^3p d^3q' \psi_{\alpha'}^*(\mathbf{p}') \phi_K^{*(-)}(\mathbf{q}, \mathbf{q}') t_\gamma \psi_\alpha(\mathbf{p}) , \quad (5)$$

where $\mathbf{p}' = \mathbf{p} + \mathbf{k} - \mathbf{q}$, and ψ is the single-particle wave function of the proton in the initial and the Λ in the final state. The wave function with the appropriate boundary conditions for the outgoing kaon of three-momentum \mathbf{q} , distorted by its interaction with the residual hypernucleus through an optical potential, is denoted by $\phi_K^{*(-)}(\mathbf{q}, \mathbf{q}')$. This wave function is generated by solving the Klein-Gordon equation using a simple $t\rho$ optical potential with the K^+N phase shifts of Ref. [36].

2.2 Basic features of the coherent kaon production process

Figure 2 compares the momentum transfer behavior with the magnitude of the differential cross section for the reaction $^{16}\text{O}(\gamma, K^+)^{16}_\Lambda\text{N}$. At 0° kaon lab angle the momentum transfer to the final hypernuclear system decreases as the photon lab energy increases. This leads to a differential cross section at $\Theta_K = 0^\circ$ which increases as E_γ increases, from around 15 nb/sr at 0.84 GeV to 330 nb/sr at 2 GeV for the particular transition shown. However, the momentum transfer increases more rapidly for non-zero kaon angles at higher photon energies. Thus, the angular distributions become more forward peaked and fall off more rapidly. The energy chosen for an experiment therefore depends on the desired result: If the goal is to perform hypernuclear spectroscopy choosing a higher photon energy around 2 GeV, while detecting the K^+ under 0° would be advantageous. If, on the other hand, one likes to extract dynamical information by mapping our transition densities via measuring angular distributions, photon energies of 1.0 to 1.2 GeV are preferable.

2.3 Extracting hypernuclear structure information

The hypernuclear production experiments over the last decades have found hypernuclear ground and excited states that can be reproduced well within the weak coupling model which assumes that the Λ couples weakly to the ground and excited states of the core nucleus. Studying these states through hypernuclear spectroscopy reveals details of the effective YN interaction in nuclear matter. Using appropriate nuclear G -matrix techniques in principle allows a self-consistent extraction of the elementary two-body YN interaction.

Figure 3 demonstrates the power of such an approach: Comparing six different Nijmegen YN potentials in hypernuclear G -matrix calculations Ref. [37] finds that for the ground state splittings of $^{11}_\Lambda\text{B}$ and $^{12}_\Lambda\text{B}$ only the NSC89, and the NSC97e and f interaction have spin-spin interactions repulsive enough to reproduce the correct ordering of the states. This finding is

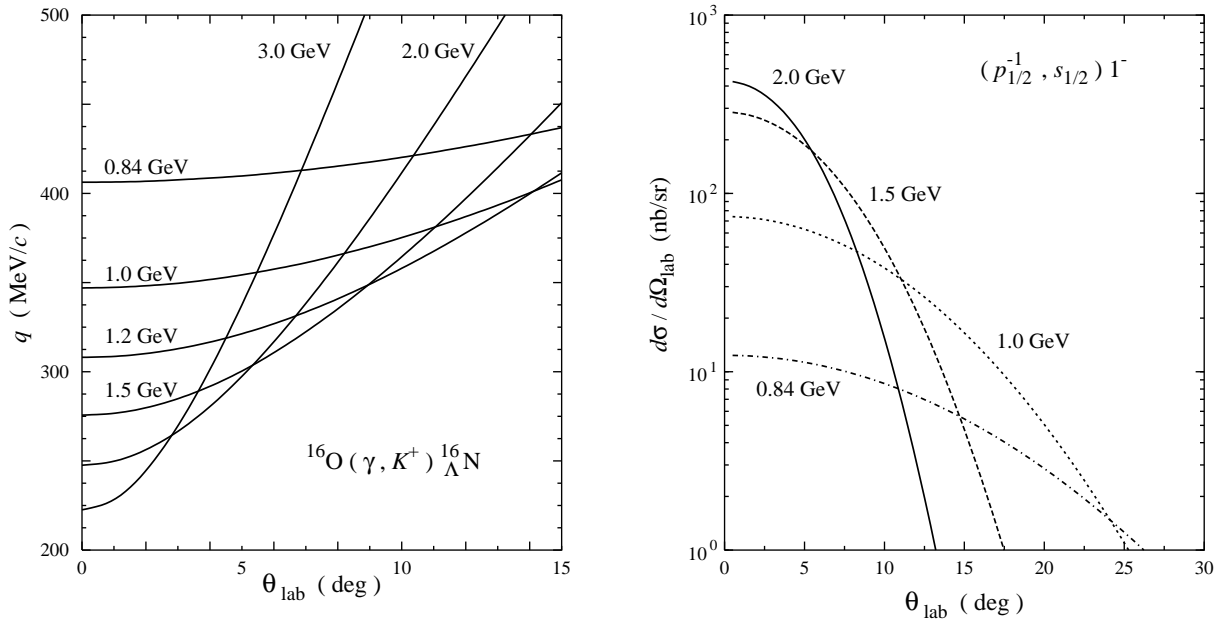


FIG. 2: Kinematic features of the (γ, K^+) process. The left side shows the momentum transfer in the lab system for several photon energies E_γ . The right side shows angular distributions for the 1^- member of the ground state doublet in $^{16}\text{O}(\gamma, K^+)^{16}_\Lambda\text{N}$ for various photon lab energies.

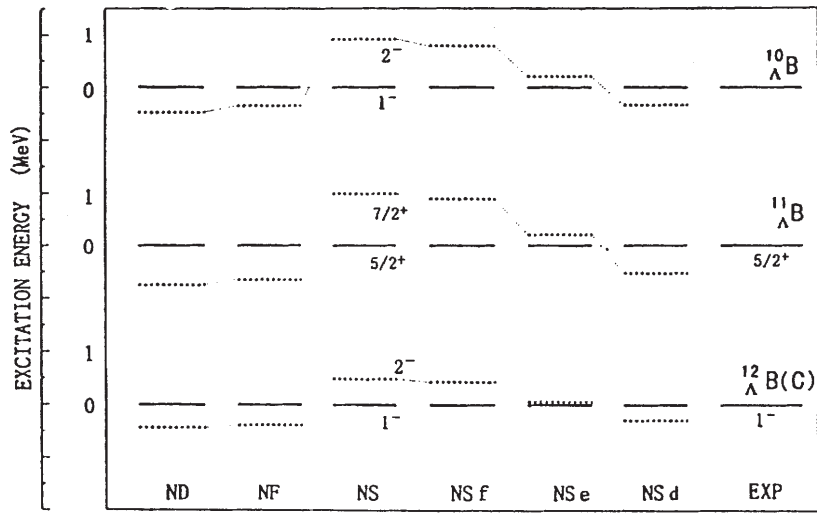


FIG. 3: Spin-doublet states in $^{10}_\Lambda\text{B}$, $^{11}_\Lambda\text{B}$, and $^{12}_\Lambda\text{B(C)}$ for the Nijmegen potentials D (ND), F (NF), NSC89 (NS), and NSC97d, e, and f, respectively. This figure is taken from Ref. [37].

supported by few-body calculations where it is found that only the above interactions can bind the hypertriton. Experimental resolution of the ground state splittings shown in Fig. 3 would allow discriminating further between those three forces. The position of higher-lying excited states is sensitive to the ΛN spin-orbit and tensor interaction.

With the exception of Refs. [6, 38] all calculations up to now have been performed in pure particle-hole configurations. These predictions may be reliable where the proton pick-up strength is not highly fragmented for stretched spin-flip transitions with maximum $J = l_N + l_\Lambda + 1$. These transitions are usually dominated by the Kroll-Ruderman $\boldsymbol{\sigma} \cdot \boldsymbol{\epsilon}$ operator and tend to have the largest cross sections. In the case shown in Fig. 2 $^{16}_\Lambda\text{N}$ is described as a pure $p_{1/2}$ proton hole coupled to an s-shell Λ , coupling to a 0^- and 1^- ground state transition. For a closed shell target nucleus in a pure particle-hole basis, the RDME simply reduce to $\Psi_{J;T}(a', a) = \delta_{ab}\delta_{a'b'}$. The degeneracy between the two ground states would be removed by including the residual ΛN interaction. For p -shell hypernuclei with the Λ in an s orbit, the $p_N s_\Lambda$ interaction can be expressed in terms of the five radial integrals \bar{V} , Δ , S_Λ , S_N , and T , assumed to be constant across the p -shell and associated with the average central, spin-spin, Λ spin-orbit, induced nucleon spin-orbit and tensor terms in the potential [39]:

$$V_{\Lambda N}(r) = V_0(r) + V_\sigma(r) \mathbf{s}_N \cdot \mathbf{s}_\Lambda + V_\Lambda(r) \mathbf{l}_{N\Lambda} \cdot \mathbf{s}_\Lambda + V_N(r) \mathbf{l}_{N\Lambda} \cdot \mathbf{s}_N + V_T(r) S_{12} . \quad (6)$$

Performing an analysis of hypernuclear structure data the “standard interaction” of Ref. [39] uses the following values (in MeV): $\Delta = 0.50$, $S_\Lambda = -0.04$, $S_N = -0.08$, and $T = 0.04$. Doublet splittings are determined mainly by the spin-spin, Λ spin-orbit, and tensor interactions Δ , S_Λ , and T , leading to the following expressions for the separation energies of the particle-hole pairs:

$$p_{3/2}s_{1/2} \quad \delta = \frac{2}{3} \Delta + \frac{4}{3} S_\Lambda - \frac{8}{5} T . \quad (7)$$

and

$$p_{1/2}s_{1/2} \quad \delta' = -\frac{1}{3} \Delta + \frac{4}{3} S_\Lambda + 8T . \quad (8)$$

This results in $\delta = 216$ keV and $\delta' = 100$ keV; thus doublet splittings are generally small. While the stretched transitions are most likely the first ones to be measured, eventually one would like to use the (γ, K^+) reaction to extract hypernuclear structure information from cases where configuration mixing is important. As discussed in Ref. [40], the reaction $^9\text{Be}(\gamma, K^+)^9_\Lambda\text{Li}$ may provide a good testing ground for resolving members of the s_Λ doublet of $3/2^+$ and $5/2^+$, coupling the s-shell Λ to the 2^+ core of ^8Li . As shown in Fig. 4, this doublet is split by 0.51 MeV according to the “standard” ΛN interaction of Ref. [39]. This splitting is mainly due to the the spin-spin part of the ΛN interaction, thus, resolving these states would provide an improved constraint. The predicted $\Delta S = 0$ RDME are large for the lower member of the doublet but small for the upper member while there is a large $\Delta J = 2$ ($\Delta S = 1$) RDME for the upper member; the two transitions would therefore produce very different angular distributions. Similar information may be extracted from the reaction $^{13}\text{C}(\gamma, K^+)^{13}_\Lambda\text{B}$.

Overall, many energy splittings of doublets with Lambdas in the s-orbit are predicted to lie well below 100 keV and may only be resolvable through additional γ -ray spectroscopy. However, a few doublet splittings, due mainly to the spin-spin force, are predicted to be around 500 keV and should be observable with kaon detectors planned for Hall A. Peaks due to s_Λ doublets based

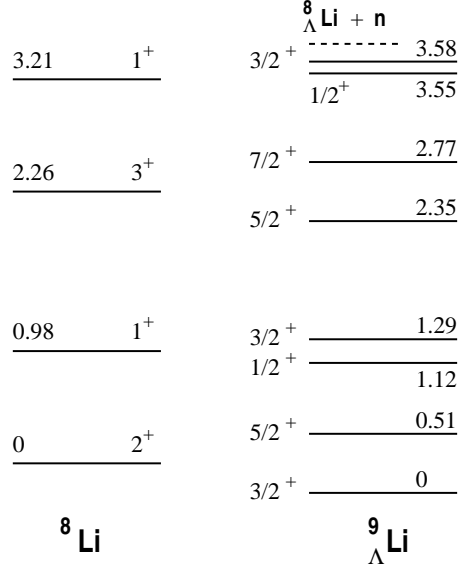


FIG. 4: The energy levels (in MeV) for ${}^8\text{Li}$ from experiment and for ${}^9_{\Lambda}\text{Li}$ calculated from the standard interaction by Millener [39]. The isospin partner ${}^9_{\Lambda}\text{Be}$ could be reached using the reaction ${}^9\text{Li}(\gamma, K^+){}^9_{\Lambda}\text{Be}$. This figure is taken from Ref. [40].

on different nuclear core states should be well separated. Furthermore, coupling p_{Λ} orbitals to nuclear core states produces a large number of excited states, predicted to be separated by several hundred keV. High resolution spectrometers for the kaons are therefore imperative in order to make progress in this field. Figure 5 demonstrates in a simulation of a planned Jlab Hall A detector the appearance of closely spaced levels with increasing experimental resolution.

2.4 Mapping out the Λ wave function in the hypernucleus

Stretched transitions of the sort $(p_{3/2,\Lambda}^{-1} s_{1/2})2^-$ or $(p_{3/2,\Lambda}^{-1} p_{3/2})3^+$ can be predicted almost model independently since they are dominated by the $\boldsymbol{\sigma} \cdot \boldsymbol{\epsilon}$ Kroll-Ruderman term. If a transition is dominated by the Kroll-Ruderman term, the operator becomes local and can be factored out of the single-particle matrix element of Eq. (5). Furthermore, neglecting kaon distortion which reduces cross sections only by about 10-20% for p -shell nuclei reduces the matrix element to

$$\langle \alpha'; K^+ | t | \alpha; \gamma \rangle = \text{const.} \int r^2 dr \psi_{\Lambda}^*(r) \psi_p(r) j_L(Qr). \quad (9)$$

Therefore, assuming one has good knowledge of the bound proton wave function from $(e, e'p)$ experiments, measuring a kaon angular distribution will be sensitive to the bound Λ wave function. Such information may prove especially valuable in certain few-body cases where adding a Λ "impurity" to the nucleus can lead to significant rearrangement of the nucleus. As discussed in detail in Ref. [42] for the $A=6$ and 7 hypernuclei, this new dynamical feature can lead to new bound states and appreciable contraction of the entire nuclear system. For example, if a Λ is added to the weakly-bound halo nucleus ${}^6\text{He}$, the predicted core-neutron rms radius decreases from 4.55 fm to 3.55 fm. The ground-state binding energies move from -0.98 MeV for ${}^6\text{He}$ (measured from the ${}^4\text{He} + 2n$ threshold) to -2.83 MeV for ${}^7_{\Lambda}\text{He}$ (predicted with respect to

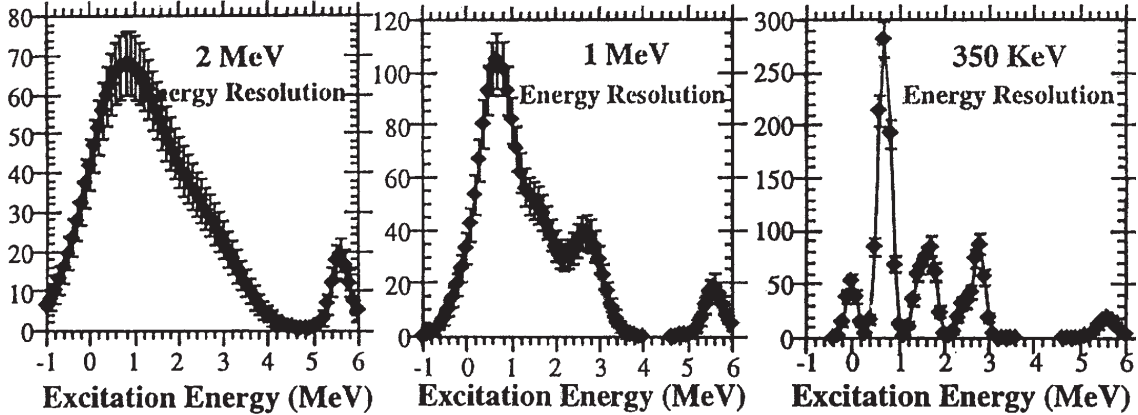


FIG. 5: Simulated excitation function for the reaction ${}^9\text{Li}(e, e'K^+){}^9_{\Lambda}\text{Be}$ with increasing experimental resolution of 2 MeV, 1 MeV, and 0.35 MeV. This figure is taken from Ref. [41].

${}^6_{\Lambda}\text{He} + n$ breakup), changing the nucleus from a Borromean to a non-Borromean system. Fig. 6 shows the density distributions of the α -core, the Λ skin and the neutron halo within ${}^7_{\Lambda}\text{He}$. Using the reaction ${}^7\text{Li}(\gamma, K^+){}^7_{\Lambda}\text{He}$ one could access this exotic hypernucleus and map out the bound state Λ wave function. This feature is unique to the (γ, K^+) process since distortion effects are minimal.

2.5 Σ hypernuclei

Little is known about the ΣN interaction and the Σ -nucleus potential. Old bubble-chamber analyses revealed a magnitude comparable to the ΛN interaction, with a significant role played by strong $\Sigma N \rightarrow \Lambda N$ conversion. First quantitative results on the Σ -nucleus potential were obtained by Σ^- atom x-ray data, yielding a potential in the nuclear center of $-(25-30)$ MeV for the real part and $-(10-15)$ MeV for the imaginary part. If such an analysis is performed with a potential nonlinear in the nuclear density the resulting real part of the Σ -nucleus potential becomes very shallow or even repulsive [43]. In this context, the formation of bound states was considered unlikely. However, to the surprise of the community, in 1980 the Saclay-Heidelberg group reported narrow structures in the unbound region of the ${}^9\text{Be}(K^-, \pi^-)$ spectrum [44]. Follow-up experiments at KEK and BNL were unable to verify this finding, except for the $A = 4$ system. Using the ${}^4\text{He}(K^-, \pi^-)$ reaction a clear signal for a ${}^4_{\Sigma}\text{He}$ bound state was observed [45, 46] with a binding energy of $E_x = 4.4$ MeV and a width of $\Gamma = 7.0$ MeV. The unique nature of this state appears to be due to the strong isospin dependence of the Σ -nucleus potential, with the $T = 1/2$ part consisting of a repulsive core and an attractive pocket near the nuclear surface. The presence of the repulsive core reduces the wave function overlap between the Σ and the residual nucleus, leading to a suppression of the $\Sigma N \rightarrow \Lambda N$ conversion width. Kaon photoproduction would allow investigating the $A = 4$ hypernuclear system via the process ${}^4\text{He}(\gamma, K^+){}^4_{\Sigma}\text{H}$. In heavy systems the isospin-independent part is expected to dominate the Σ -nucleus potential. Shown in Fig. 7 is a calculation by Ref. [47], predicting an attractive potential in the nuclear interior with a repulsive bump near the surface. Combing such a strong potential with the Coulomb potential can produce narrow structures, as shown in the right panel of Fig. 7. While the predictions of Ref. [47] shown in Fig. 7 were obtained using the (π^-, K^+) reaction,

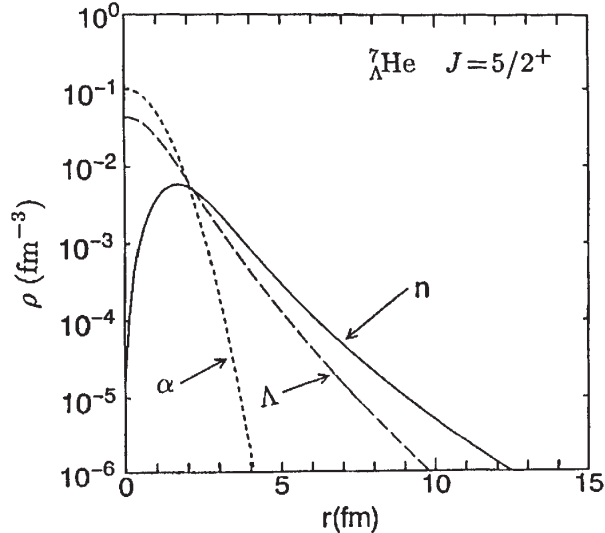


FIG. 6: Density distributions of the valence nucleon and Λ in the weakly bound state of ${}^7_{\Lambda}\text{He}(5/2^+)$. The radius r is measured from the ${}^5_{\Lambda}\text{He}$ cm frame. This figure is taken from Ref. [42].

we propose to rather photoproduce such Coulomb-assisted Σ -hypernuclear bound states through reactions such as ${}^{208}\text{Pb}(\gamma, K^+)_{\Sigma^-}{}^{208}\text{Tl}$. This would eliminate the need for a strongly absorbed pion in the initial state and open the possibility to populate deeply bound Σ -hypernuclear states. Again, high-resolution detectors are imperative for this kind of second-generation experiment.

2.6 A special case: Photoproduction of the hypertriton

In the periodic table of hypernuclei, the hypertriton, a bound state consisting of a proton, a neutron, and a lambda, holds a special place as the lightest hypernucleus. Since neither the ΛN nor the ΣN interactions are sufficiently strong to produce a bound two-body system with $S = -1$, the hypertriton is the first system in which the YN force, including the interesting Λ - Σ conversion potential, can be tested in the nuclear environment. Therefore, the hypertriton plays an important role in hypernuclear physics, similar to the deuteron in nuclear physics. Ref. [48] has carried out a detailed investigation of this system using Faddeev equations and found that binding the hypertriton with its small binding of 130 keV (with respect to $\Lambda - d$ break-up), requires a fine-tuning of the YN 1S_0 amplitude which is found in only few potentials, such as the NSC89[49]. While this feature makes the hypertriton a fascinating system to study, it is precisely the weak binding that makes this loosely bound system, which displays halo-like features similar to neutron-rich nuclei near the neutron drip line, a difficult system to produce in high-momentum reactions such as ${}^3\text{He}(\gamma, K^+)_{\Lambda}{}^3\text{H}$.

In contrast to the transition matrix elements for p -shell hypernuclei [Eq. (3)], the nuclear matrix elements for the process on ${}^3\text{He}$ do not separate into a many-body nuclear structure part and a single-particle one-body integral, but they are evaluated straightforwardly in terms of an integral over all internal momenta and states contributing to the process [50],

$$T_{\text{fi}} = \langle {}^3_{\Lambda}\text{H} | t^{\gamma p \rightarrow K^+ \Lambda} | {}^3\text{He} \rangle,$$

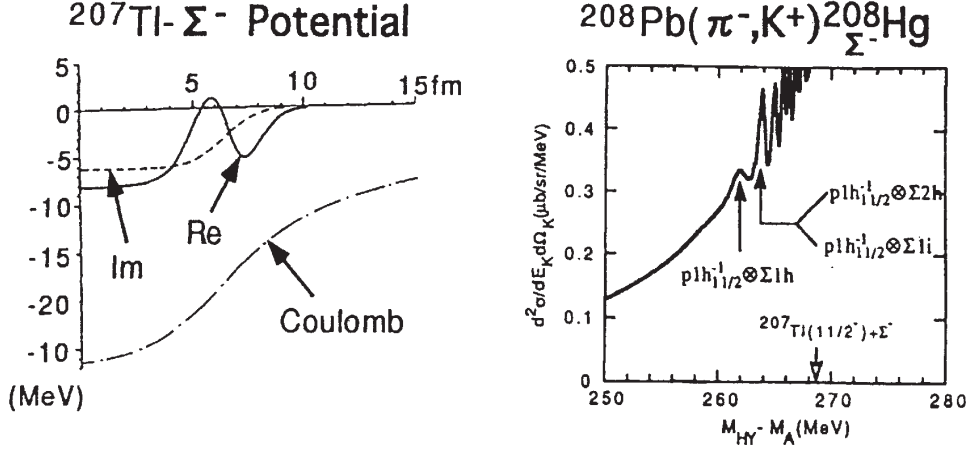


FIG. 7: Calculated Σ -Tl potential (left) and the $^{208}\text{Pb}(\pi^-, K^+)^{208}\text{Hg}$ spectrum produced with the (π^-, K^+) reaction. This figure is taken from Ref. [47].

$$= \left(\frac{E_{3\text{He}} E_{\Lambda}^3}{M_{3\text{He}} M_{\Lambda}^3} \right)^{1/2} \int d^3\mathbf{p} d^3\mathbf{q} \left(\frac{m_f m_i}{E_f E_i} \right)^{1/2} \Psi_{\Lambda}^3(\mathbf{p}, \mathbf{q}') t^{\gamma p \rightarrow K\Lambda}(\mathbf{q}, \mathbf{Q}) \Psi_{3\text{He}}(\mathbf{p}, \mathbf{q}), \quad (10)$$

In order to estimate the magnitude of the production cross section one may consider the struck nucleon inside ^3He as having a fixed momentum [51]. In this case, the elementary operator can be factored out of the integral and the cross section off ^3He may be written as

$$\frac{d\sigma_{\text{T}}}{d\Omega_K} = \frac{1}{9} W_A^2 |F(Q)|^2 \left(\frac{d\sigma_{\text{T}}}{d\Omega_K} \right)_{\text{proton}}, \quad (11)$$

with the nuclear form factor

$$F(Q) = \int d^3\mathbf{q} d^3\mathbf{p} \Psi_{\Lambda}^3(\mathbf{p}, \mathbf{q} + \frac{2}{3}\mathbf{Q}) \Psi_{3\text{He}}(\mathbf{p}, \mathbf{q}), \quad (12)$$

As shown in Fig. 8, using the nuclear form factor of Eq. (12) reduces the reaction cross section of Eq. (11) by two orders of magnitude compared to the elementary reaction. As $\theta_K^{\text{c.m.}}$ increases, the cross section drops quickly, since the nuclear momentum transfer increases rapidly as function of $\theta_K^{\text{c.m.}}$ (see Fig. 2). Figure 8 also shows the significant difference between the cross sections calculated with the approximation of Eq. (11) and the full result obtained from Eq. (10). This discrepancy is due to the ‘‘factorization’’ approximation, since the integrations of both spin-independent and spin-dependent amplitudes over the internal momentum weighted by the two wave functions lead to destructive interference and further reduce the cross section. The cross section for kaon photoproduction is in fact very small, of the order of about 1 nb/sr at most, and even smaller for larger kaon angles. The underlying reason is the lack of high momentum components in the $^3_{\Lambda}\text{H}$ wave function, inhibiting hypernuclear formation. Nevertheless, the electromagnetic production of the hypertriton has to be compared to the production with strong probes, e.g. $d(p, K^+)^3_{\Lambda}\text{H}$ whose cross sections also have been predicted to be around 1 nb/sr [52]. As shown in Fig. 9, S -waves alone are insufficient to describe the reaction. Inclusion of the higher partial waves further reduce the cross section by a factor of more than three. This can be traced

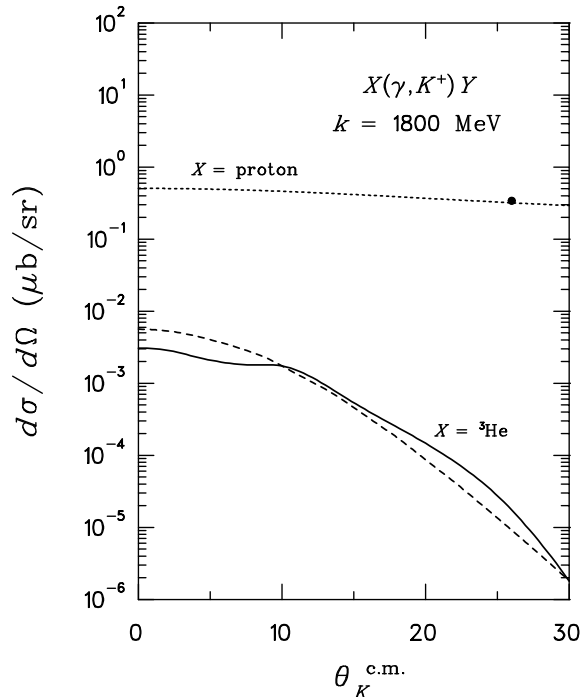


FIG. 8: Differential cross section for kaon photoproduction off the proton and ${}^3\text{He}$ as function of kaon angle. The elementary reaction (dotted line) is taken from Ref. [2] and the corresponding experimental datum is from Ref. [56]. The dashed line shows the approximation for production off ${}^3\text{He}$ calculated from Eq. (11), the solid line represents the exact calculation using S -waves. The figure is taken from Ref. [50].

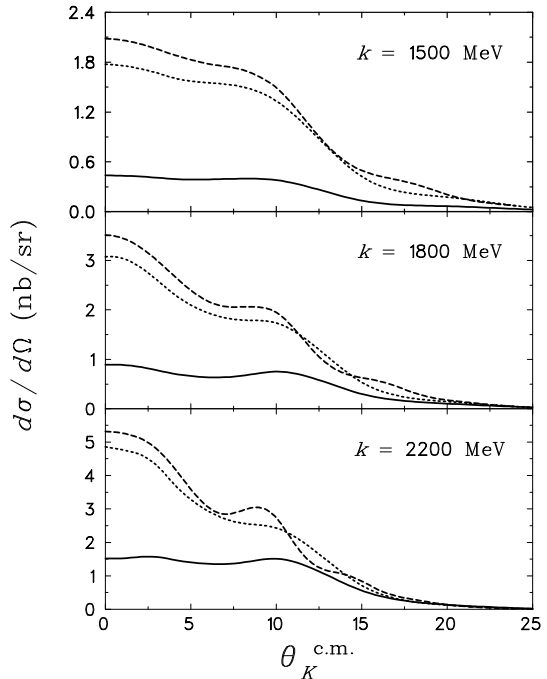


FIG. 9: The cross section for kaon photoproduction off ${}^3\text{He}$ at three different excitation energies. The dotted curves are obtained from the calculation with S -waves only and the simple hypertriton wave function, the dashed curves are obtained with S -waves only and the correlated Faddeev wave function of Ref. [48], while the solid curves show the result after using all of the partial waves and the simple hypertriton wave function[54]. The figure is taken from Ref. [50].

to an overlap of D -wave components in the ${}^3\text{He}$ wave function with the dominant S -wave in the hypertriton. In comparison, the higher partial waves in pion photo- and electroproduction[53] decrease the cross section by at most 20%. Fig. 9 also compares calculations with S -waves using both a simple analytical model for the hypertriton wave function [54] and a correlated three-body Faddeev wave function [48] that includes the proper short-range behavior. While the cross sections obtained with the Faddeev wave functions does show more structure, the difference in magnitude are only of order 10 - 20%. Calculations coming up on ${}^4_{\Lambda}\text{He}$ and ${}^4_{\Lambda}\text{H}$ [55] will supplement these studies on ${}^3_{\Lambda}\text{H}$ and, because of their richer spectra, will allow an even closer examination of the YN force.

3 QUASIFREE KAON PRODUCTION

Due to the sizable momentum transfer to the hypernuclear system the probability of forming such bound states is in fact rather small. Ref. [33] has estimated this formation probability to be

around 5-10% of the total (γ, K^+) strength on nuclear targets, thus most of the kaon production events will come from quasifree production, $A(\gamma, KY)B$, where the kaon can be a K^+ or K^0 , and the hyperon can be either a Λ or a Σ .

3.1 Quasifree kaon production on the deuteron

In order to explore the YN force more directly, hyperon production processes on the deuteron, such as $\gamma(d, K^+)YN$, appear as natural candidates. The hope is that the pole structure of the YN scattering operator will have visible effects in such a production process. In a recent study [57] the S -matrix pole structure for the YN system has been investigated for various presently used YN forces. As is well known there is no bound state in the $\Lambda(\Sigma)N$ system, but the present potential models support poles of the S -matrix which are close to the Λ and Σ thresholds. Near the Λ threshold there are two S -wave virtual states at about -3 and -5 MeV, and close to the Σ threshold there is a ${}^3S_1 - {}^3D_1$ pole which appears at different unphysical sheets of the Riemann energy surface depending on the potential used. This pole causes cusp-like structures in the ΛN scattering at the Σ threshold. Their forms and strengths depend on the potential employed.

Pioneering work in inclusive and exclusive K^+ photoproduction on the deuteron has been done before [58] based on simple hyperon-nucleon forces. These calculations suggested that significant YN final-state interaction effects be present near the production thresholds. Recently, these results were reexamined [59] using various recently formulated YN forces [49, 60] together with realistic NN forces and an updated elementary photoproduction operator of the K^+Y pair on a nucleon. For kaon photoproduction on the deuteron the nuclear matrix element can be conveniently rewritten by applying the Möller wave operator generating the final scattering state to the right:

$$\langle \Psi_{\mathbf{q}_Y \mu_Y \nu_Y \mu_N \nu_N}^{(-)} | t_{\gamma K}(1) | \Phi_{d\mu_d} \rangle \equiv \langle \mathbf{q}_Y \mu_Y \nu_Y \mu_N \nu_N | T_Y | \Psi_{d\mu_d} \rangle \quad (13)$$

Since we allow for $\Lambda - \Sigma$ conversion the state $\langle \Psi_{\mathbf{q}_Y \mu_Y \nu_Y \mu_N \nu_N}^{(-)} |$ as well as the corresponding free state $\langle \mathbf{q}_Y \mu_Y \nu_Y \mu_N \nu_N |$ is a row with a Λ and a Σ component. The operator T_Y applied to the deuteron state obeys the integral equation

$$T_Y | \Psi_{d\mu_d} \rangle = t_{\gamma K}^Y(1) | \Psi_{d\mu_d} \rangle + \sum_{Y'} V_{Y, Y'} G_0^{Y'} T_{Y'} | \Psi_{d\mu_d} \rangle \quad (14)$$

Equation (14) contains the elementary operator $t_{\gamma K}^Y$ producing a specific hyperon Y and $V_{Y, Y'}$ is the hyperon-nucleon force including $\Lambda - \Sigma$ conversion.

Figure 10 compares inclusive cross sections for $d(\gamma, K^+)$ in plane wave impulse approximation (PWIA) with calculations that include FSI generated with the hyperon-nucleon forces NSC89 [49] and NSC97f [60] which both lead to the correct hypertriton binding energy. The two pronounced peaks around $p_K = 945$ and 809 MeV/c can be understood in PWIA. They are due to quasi-free processes, where one of the nucleons in the deuteron is a spectator and has zero momentum in the lab system. This then leads to a vanishing argument $q = 0$ in the deuteron wavefunction, which causes the peaks. Under this condition the kinematics of the γ -induced process on a single nucleon fixes the peak positions for p_K in the lab system. Figure 10 shows significant deviations between the plane wave result and the results with FSI based on the NSC89 and NSC97f hyperon-nucleon forces. Near the $K^+\Lambda N$ threshold the FSI enhances the cross section by up to 90%. Near the $K^+\Sigma N$ threshold the effects are even more dramatic.

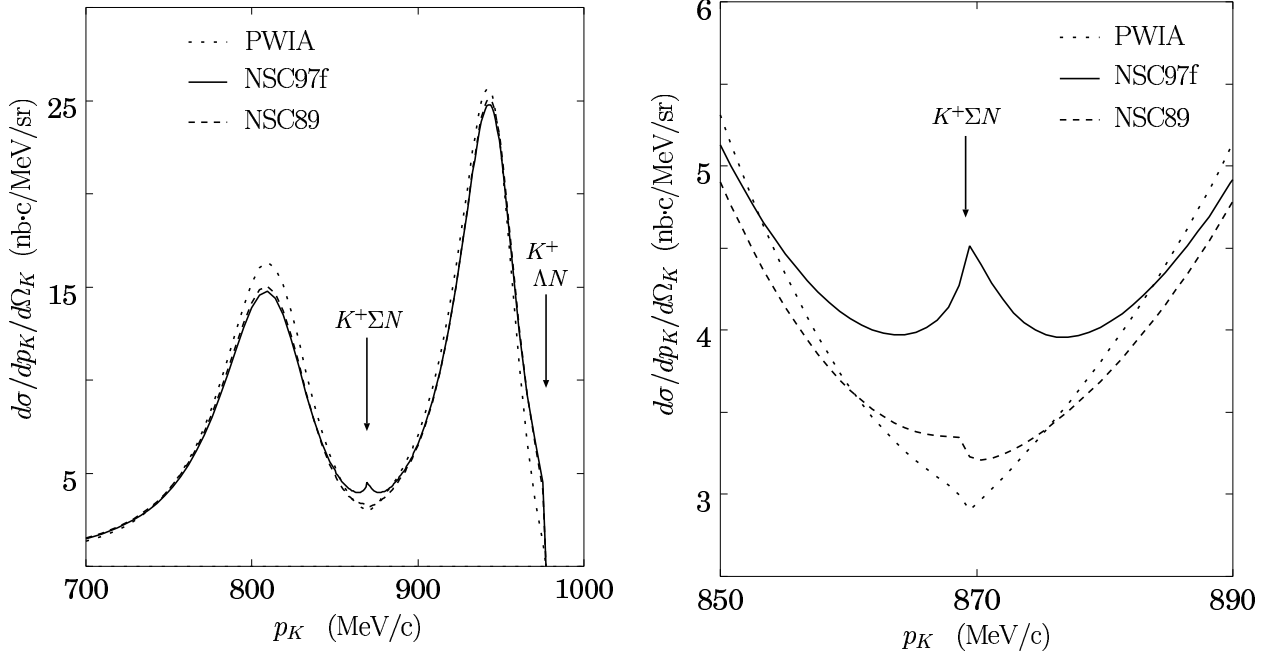


FIG. 10: The left side shows the inclusive $\gamma(d, K^+)$ cross section as a function of lab momenta p_K for $\theta_K = 0^\circ$ and photon lab energy $E_\gamma = 1.3$ GeV. The plane wave result is compared to two YN force predictions. The FSI effects are especially pronounced near the $K^+\Lambda N$ and $K^+\Sigma N$ thresholds (see the enlarged figure on the right side), the locations of which are indicated by the arrows. The right side shows the results enlarged around the $K^+\Sigma N$ threshold. The figures are taken from Ref. [59].

While NSC89 slightly enhances the cross section, NSC97f leads to a much stronger effect with a prominent cusp-like structure. The two YN potentials lead to predictions which differ by up to 35%. This can be traced back to the location of the S -matrix pole for the $\Lambda N - \Sigma N$ system around the ΣN threshold. Each of the two YN potentials generate a pole in the state ${}^3S_1 - {}^3D_1$ near $p_{\Sigma N} = 0$. The potential NSC89 leads to a pole position which in a single channel case would be called a virtual state (in this case it would lie exactly on the imaginary axis). The coupling of the Λ and Σ channels moves the pole for the NSC97f force away from the positive imaginary axis into the second $p_{\Sigma N}$ quadrant. In a time-dependent description the energy related to that pole position leads to a decreasing amplitude. In the literature, this sort of pole is sometimes referred to as an ‘unstable bound state’. Apparently, the actual pole position depends on the details of the YN force. The pole positions are an inherent property of the YN forces and the actual location chosen by nature should be determined with the help of experimental measurements.

3.2 Quasifree kaon production on heavier nuclei

Quasifree production on heavier nuclei allows for the study of the reaction process in the nuclear medium as well as final state interaction effects without being obscured by the details of the nuclear transitions as discussed above. The predictions presented here [61] are in a DWIA framework that has been successfully applied in previous work on quasifree pion photo- and electroproduction [62] and eta photoproduction on nuclei [63]. The key ingredients are:

1. the single-particle wave function and spectroscopic factor, usually taken from electron scattering,
2. the elementary kaon photoproduction amplitude,
3. the distorted kaon wave function which can be taken from kaon elastic scattering in case of the K^+ ,
4. the hyperon-nucleus final-state interaction.

In contrast to hypernuclear production discussed above, the reaction is *quasifree*, meaning that the magnitude of Q has a wide range, including zero. Since the reaction amplitude is proportional to the Fourier transform of the bound state single particle wavefunction, it falls off quickly as the momentum transfer increases. Thus, we will restrict ourselves to the low Q region (< 500 MeV/c) where the nuclear recoil effects can be safely neglected for nuclei of $A > 6$. The nuclear structure aspects are now contained in the spectroscopic factor, and in the single-particle matrix element of Eq. (5) the bound-state Λ wave function has to be replaced by a scattering state, obtained from solving a Schrodinger equation with some optical potential.

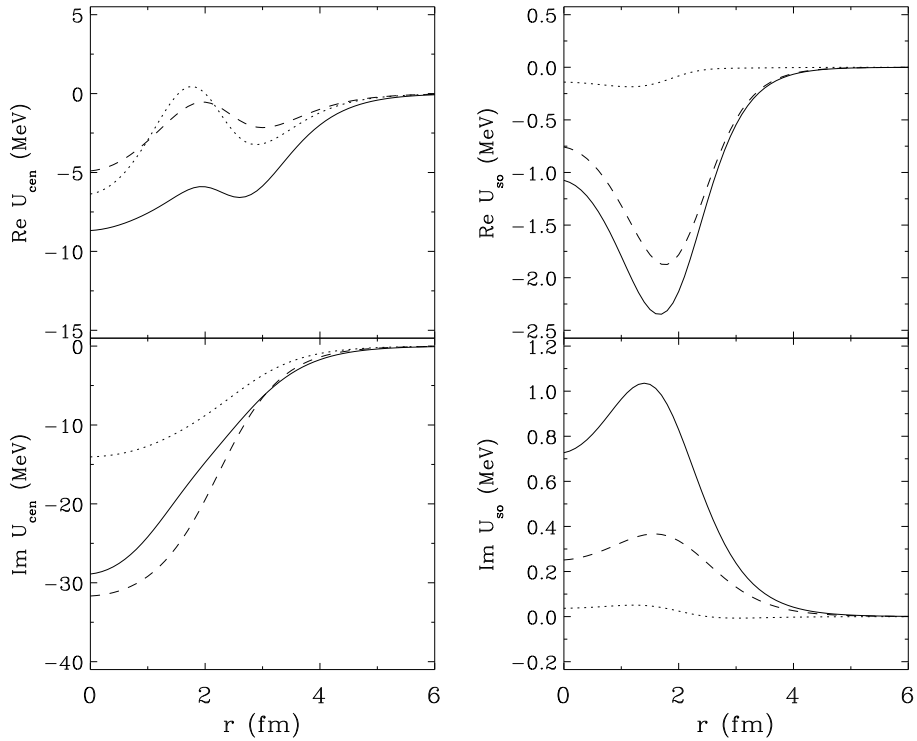


FIG. 11: Hyperon optical potentials for ^{12}C at 200 MeV kinetic energy. The dotted line shows the Λ potential, while the dashed line depicts the Σ^0 potential. The proton potential (solid line) is shown for comparison.

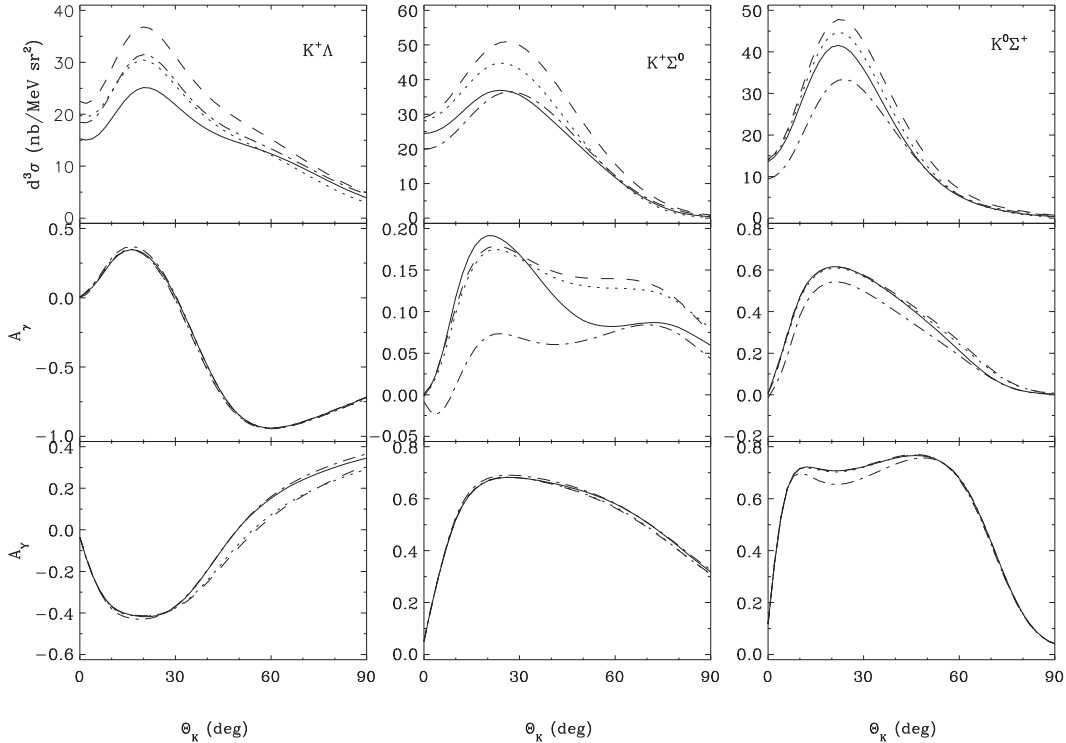


FIG. 12: Results for the differential cross section, the polarized photon asymmetry, and the hyperon recoil polarization for the reaction $^{12}\text{C}(\gamma, KY)\text{B}_{\text{g.s.}}$ at $E_\gamma=1.4$ GeV and $Q = 120$ MeV/c under quasifree kinematics. Three of the six possible channels are shown in the three columns. The four curves correspond to calculations in PWIA (dashed), in DWIA with kaon only distorted (dotted), with hyperon only distorted (dash-dotted), and with both distorted (solid).

3.3 Hyperon-nucleus optical potentials

Very few optical potentials have been constructed for the Λ and Σ , mostly due to lack of data. Here, we employ the global optical model of Ref. [64]. It is based on a global nucleon-nucleus Dirac optical potential fit [65]. The parameters of the potential are motivated by the constituent quark model and adjusted to fit the hypernuclear binding energy data. We use its nonrelativistic equivalent version which has a central and a spin-orbit part, $U(r) = U_{\text{cen}}(r) + U_{\text{so}}(r) \boldsymbol{\sigma} \cdot \mathbf{l}$. Note that the spin-orbit part is multiplied by a factor that depends on the partial wave under consideration. Fig. 11 shows the real and imaginary parts of both $U_{\text{cen}}(r)$ and $U_{\text{so}}(r)$ on ^{12}C at 200 MeV kinetic energy for the Λ and the Σ^0 . For comparison, they are also shown for the proton. The real parts of the central potential are clearly smaller than the proton potential by around a factor of two, reflecting the fact that Lambdas and Sigmas have a smaller binding energy in hypernuclei. The imaginary part of the Σ 's central potential is similar in magnitude to that of the nucleon, due to the large $\Sigma N \rightarrow \Lambda N$ conversion width. The very small spin-orbit potential of the Λ is a reflection of the ΛN spin-orbit force which is known to be small.

Results are shown in Fig. 12 for the reaction $^{12}\text{C}(\gamma, KY)^{11}\text{B}_{\text{g.s.}}$ at $E_\gamma=1.4$ GeV and $Q = 120$ MeV/c under quasifree kinematics. As the kaon angle increases, the kaon energy decreases while the hyperon energy increases. In this particular case, the kaon and hyperon energies

can reach around 500 to 700 MeV. Figure 12 shows the differential cross sections as well as two polarization observables, comparing PWIA calculations with results that include hyperon and kaon final state interaction (FSI). Kaon distortion reduces the cross sections by about 10-20% but has little effect on the polarization observables. Including the hyperon FSI reduces the angular distributions by up to 30% at forward angles. Again, with the exception of the photon polarization in $K^+\Sigma^0$ production, the polarization observables are barely affected by the inclusion of FSI. This situation is similar to previous findings in quasifree pion and eta photoproduction [62, 63]. It opens the possibility to use the polarization observables as a way to study modifications of the basic production process in the nuclear medium. The magnitudes of the Σ and P observables is sizeable and should be measurable.

4 CONCLUSIONS

Driven by new experimental results from facilities like Jlab and ELSA, the field of Strangeness production with photons and electrons is experiencing a revival. Experimental proposals, some approved at Jlab over ten years ago, are being carried out and begin to produce data of unprecedented quality. In the meantime, our understanding of the elementary production mechanism has evolved significantly over the last decade. Within effective Lagrangian approaches the need for hadronic form factors has become clear, along with their implications for gauge invariance. Born coupling constants, long found to be too small in model fits, can now be reconciled with their SU(3) values and upcoming high-quality data should allow extracting their precise values by extrapolating to a Born pole using dispersion relations. In the resonance sector new coupled-channels analyses are beginning to shed light on the relevant resonances by combining data from kaon photoproduction with information from hadronic strangeness production and with the vast reservoir of data in pion scattering and pion photoproduction. Attempts to describe threshold production through Chiral Perturbation Theory are still in their infancy but may eventually lead to a better understanding of the validity of chiral expansions in the SU(3) sector. With our knowledge of the elementary kaon production amplitude expanding, predictions for kaon productions on nuclear targets are becoming more reliable. Here the few-body sector is especially appealing due to the rigor of the theoretical calculations. Modern hyperon-nucleon forces can be studied directly in quasifree kaon production on the deuteron. The $A = 3$ and 4 hypernuclei can now be handled theoretically without approximations and, using the nucleus as a spin-isospin filter, place severe constraints on certain parts of the YN interaction. Jlab experiments are just beginning to take advantage of the photoproduction mechanism to excite unnatural parity and high-spin states; this spectroscopic information will supplement our knowledge of the effective ΛN interaction from present hadronic probes employed at KEK and BNL. The full power of the almost distortionless (γ, K^+) reaction to populate deeply bound states in heavier nuclei and study details of the Λ wave function will hopefully be used in second-generation experiments at Jlab and MAMI C. In the coming years, these experimental and theoretical developments should lead to a much improved understanding not only of the YN -force, but also of hadronic physics in the SU(3) realm in general.

Acknowledgements

C.B., H.H., F.X.L., and L.E.W. acknowledge the support from the US Department of Energy. W.G. and L.T. would like to thank the Deutsche Forschungsgemeinschaft for financial support.

S.S.K. thanks the Heisenberg-Landau program for support. T.M. acknowledges support from the Deutscher Akademischer Austauschdienst (DAAD). C.B., T.M. and S.S.K. are grateful for the hospitality of the Insitut für Kernphysik at the University of Mainz.

References

- [1] J.C. David, C. Fayard, G.H. Lamot, and B. Saghai, Phys. Rev. C **53**, 2613 (1996).
- [2] R.A. Williams, C.-R. Ji, and S.R. Cotanch, Phys. Rev. C **46**, 1617 (1992).
- [3] T. Mart, C. Bennhold, and C.E. Hyde-Wright, Phys. Rev. C **51**, R1074 (1995); T. Mart, Phys. Rev. C **62**, 038201 (2000).
- [4] B. S. Han, M. K. Cheoun, K. S. Kim, and I.-T. Cheon, nucl-th/9912011.
- [5] C. Bennhold and L.E. Wright, Phys. Rev. C **39**, 927 (1989); Phys. Lett. B **191**, 11 (1987); Prog. Part. Nucl. Phys. **20**, 377 (1988).
- [6] A.S. Rosenthal, D. Halderson, K. Hodgkinson, and F. Tabakin, Ann. Phys. (NY) **184**, 33 (1988); A.S. Rosenthal, D. Halderson, and F. Tabakin, Phys. Lett. B **182**, 143 (1986);
- [7] T. Feuster and U. Mosel, Phys. Rev. C **58**, 457 (1998).
- [8] T. Feuster and U. Mosel, Phys. Rev. C **59**, 460 (1999).
- [9] A. Waluyo, C. Bennhold, H. Haberzettl, G. Penner, U. Mosel and T. Mart, in *Proceedings of the 18th Indonesian National Symposium*, Jakarta, Indonesia, April 2000 (in press), nucl-th/0008023.
- [10] R.A. Adelseck and B. Saghai, Phys. Rev. C **42**, 108 (1990); Phys. Rev. C **45**, 2030 (1992).
- [11] J. Antolin, Z. Phys. C **31**, 417 (1986).
- [12] R.G.E. Timmermans *et. al.*, Nucl. Phys. **A585**, 143c (1995).
- [13] S. Choe, M.K. Cheoun, and S.H. Lee, Phys. Rev. C **53**, 1363 (1996)
- [14] T.M. Aliev and M. Savci Phys. Rev. C **61**, 045201 (2000).
- [15] B.B. Deo and A.K. Bisoi, Phys. Rev. D **9**, 288 (1974).
- [16] H. Haberzettl, Phys. Rev. C **56**, 2041 (1997).
- [17] H. Haberzettl, C. Bennhold, T. Mart, and T. Feuster, Phys. Rev. C **58**, R40 (1998).
- [18] L. Tiator, C. Bennhold and S.S. Kamalov, Nucl. Phys. A **580**, 455 (1994).
- [19] R.A. Adelseck and L.E. Wright, Phys. Rev. C **38**, 1965 (1988).
- [20] M. Guidal, J.M. Laget, and M. Vanderhaeghen, Nucl. Phys. A **627**, 645 (1997).
- [21] T.P. Vrana, S.A. Dytman, and T.-S.H. Lee, Phys. Rep. **328**, 181 (2000).

- [22] D.M. Manley, E.M. Saleski, Phys. Rev. D **45**, 4002 (1992).
- [23] K. W. Bell *et al.*, Nucl. Phys. **B222**, 389 (1983).
- [24] D. H. Saxon *et al.*, Nucl. Phys. **B162**, 522 (1980).
- [25] SAPHIR Collaboration: M. Q. Tran *et al.*, Phys. Lett. B **445**, 20 (1998).
- [26] C. Caso *et al.*, Eur. Phys. J. C **3**, 1 (1998).
- [27] S. Capstick and W. Roberts, Phys. Rev. D **49**, 4570 (1994).
- [28] S. Capstick and W. Roberts, Phys. Rev. D **58**, 074011 (1998).
- [29] T. Mart and C. Bennhold, Phys. Rev. C **61**, 012201(R) (1999); C. Bennhold *et al.*, nucl-th/0008024.
- [30] S. Capstick, Phys. Rev. D **46**, 2864 (1992).
- [31] D. Drechsel, O. Hanstein, S.S. Kamalov, L. Tiator, Nucl. Phys. **A645**, 145(1999).
- [32] Jefferson Lab Hall C experiment 89-009, E.V. Hungerford and L.G. Tang, spokespersons.
- [33] S.R. Cotanch and S.S. Hsiao, Nucl. Phys. **A450**, 419c (1986).
- [34] J. Cohen, Phys. Rev. C **32**, 543 (1985); Intern. J. of Mod. Phys. A **4**, 1 (1989).
- [35] H. Bando, T. Motoba, and J. Zofka, Intern. J. Mod. Phys. **A5**, 4021 (1990).
- [36] B.R. Martin, Nucl. Phys. **B94**, 413 (1975).
- [37] Y. Yamamoto, in *Proceedings of the Sendai International Workshop on the Spectroscopy of Hypernuclei*, Sendai, Japan, January 8-10, 1998, p. 174.
- [38] T. Motoba, M. Sotona, and K. Itonaga, Prog. Theor. Phys. Suppl. **117**, 123 (1994).
- [39] D.J. Millener *et al.*, Phys. Rev. C **31**, 499 (1985).
- [40] C.B. Dover and D.J. Millener, in *Modern Topics in Electron Scattering* (World Scientific, Singapore, 1990, B. Frois and I. Sick, eds.)
- [41] Jefferson Lab Hall A experiment 94-107, S. Frullani, F. Garibaldi and P. Markowitz, spokespersons.
- [42] E. Hiyama *et al.*, Phys. Rev. C **53**, 2075 (1996).
- [43] C.J. Batty *et al.*, Phys. Lett **B335**, 273 (1994).
- [44] R. Bertini *et al.*, Phys. Lett. **B90**, 375 (1980).
- [45] R.S. Hayano *et al.*, Phys. Lett. **B231**, 355 (1989).
- [46] T. Nagae *et al.*, Phys. Rev. Lett. **80**, 1605 (1998).
- [47] S. Tadokoro and Y. Akaishi, Phys. Lett. **B282**, 19 (1992).

- [48] K. Miyagawa, H. Kamada, W. Glöckle, and V. Stoks, Phys. Rev. C **51**, 2905 (1995).
- [49] P.M.M. Maessen, Th.A. Rijken, and J.J. de Swart, Phys. Rev. C **40**, 2226 (1989).
- [50] T. Mart, L. Tiator, D. Drechsel and C. Bennhold, Nucl. Phys. **A640**, 235 (1998).
- [51] S. S. Kamalov, L. Tiator, and C. Bennhold, Phys. Rev. C **47**, 941 (1993); and references therein.
- [52] V.I. Komarov, A.V. Lado, and Yu.N. Uzikov, J. Phys. G **21**, L69 (1995).
- [53] L. Tiator, A.K. Rej, and D. Drechsel, Nucl. Phys. **A333**, 343 (1980); L. Tiator, Nucl. Phys. **A364**, 189 (1981).
- [54] J. G. Congleton, J. Phys. G **18**, 339 (1992).
- [55] E. Hiyama *et al.*, Nucl. Phys. **A639**, 169c (1998).
- [56] P. Feller *et al.*, Nucl. Phys. B **39**, 413 (1972).
- [57] K. Miyagawa and H. Yamamura, Phys. Rev. **C60**, 024003 (1999).
- [58] R.A. Adelseck and L.E. Wright, Phys. Rev. C **39**, 580 (1989); X. Li and L.E. Wright, J. Phys. G: Nucl. Part. Phys. **17**, 1127 (1991).
- [59] H. Yamamura, K. Miyagawa, T. Mart, C. Bennhold and W. Glockle, Phys. Rev. C **61**, 014001 (2000).
- [60] Th.A. Riken, V.G.J. Stoks, and Y. Yamamoto, Phys. Rev. C **59**, 21 (1999).
- [61] F.X. Lee *et al.*, nucl-th/9907119.
- [62] X. Li (F.X. Lee), L.E. Wright, and C. Bennhold, Phys. Rev. C **48**, 816 (1993); Phys. Rev. C **50**, 1283 (1994).
- [63] F.X. Lee, L.E. Wright, C. Bennhold, L. Tiator, Nucl. Phys. **A603**, 345 (1996).
- [64] E.D. Cooper, B.K. Jennings and J. Mareš, Nucl. Phys. **A580**, 419 (1994); Nucl. Phys. **A585**, 157 (1995).
- [65] E.D. Cooper, S. Hama, B.C. Clark, and R.L. Mercer, Phys. Rev. C **47**, 297 (1993).